

Article

Quantum Chemical Approaches to the Encapsulation of Parathion, Chlorpyrifos and Coumaphos by Armchair and Zigzag Boron Nitride Nanotubes Doped with Aluminum

Rong-Lieh Wang and Chia Ming Chang * 

Environmental Molecular and Electromagnetic Physics (EMEP) Laboratory, Department of Soil and Environmental Sciences, National Chung Hsing University, Taichung 40227, Taiwan; 4109039054@smail.nchu.edu.tw

* Correspondence: abinitio@dragon.nchu.edu.tw

Abstract: Boron nitride nanotubes have been widely used as drug delivery vehicles and for the controlled release of targeted therapeutic drugs. In this study, we calculated the encapsulation efficiencies of three organophosphorus pesticides, parathion, chlorpyrifos, and coumaphos, using quantum chemical methods. The results show that the encapsulation energy of zigzag BNNT(20,0) is lower than that of armchair BNNT(12,12) to encapsulate parathion. Al doping helps to decrease the encapsulation energy and Al-doped zigzag BNNT(20,0) + parathion has the greatest binding affinity. In addition, the energy gap of armchair BNNT(12,12) encapsulating organophosphorus pesticides changed significantly. Al doping reduces the band gap of boron nitride nanotubes. Al-doped armchair BNNT(12,12) has the strongest electron-accepting ability and is a promising sensor material.

Keywords: boron nitride nanotube; organophosphorus pesticide; encapsulation; controlled release; quantum chemical method



Citation: Wang, R.-L.; Chang, C.M. Quantum Chemical Approaches to the Encapsulation of Parathion, Chlorpyrifos and Coumaphos by Armchair and Zigzag Boron Nitride Nanotubes Doped with Aluminum. *Crystals* **2023**, *13*, 685. <https://doi.org/10.3390/cryst13040685>

Academic Editors: Sergio Brutti and Thomas M. Klapötke

Received: 23 March 2023

Revised: 7 April 2023

Accepted: 14 April 2023

Published: 17 April 2023



Copyright: © 2023 by the authors. Licensee MDPI, Basel, Switzerland. This article is an open access article distributed under the terms and conditions of the Creative Commons Attribution (CC BY) license (<https://creativecommons.org/licenses/by/4.0/>).

1. Introduction

Boron nitride nanotubes (BNNTs) and carbon nanotubes (CNTs) share similar structural features and physical properties, with the most notable difference being that BNNTs have a large energy gap of approximately 5.5 eV [1,2]. Today, the application of boron nitride materials spans many fields. Among them, BNNTs are widely used in electronic materials, adsorbents, and sensors, and have served as a drug carrier for targeted therapy in the field of biomedicine [3]. BNNTs have high structural stability and chemical inertness. In the field of semiconductors, BNNTs have good processability, and the energy gap can be reduced by doping metal atoms [4]. In addition, BNNTs are non-toxic and have excellent biocompatibility, so they are suitable for drug delivery and controlled release [5,6].

The physical and chemical properties of BNNTs are influenced by their diameter. The larger the diameter, the weaker the restraint and the better the stability. There have been many studies using the diameter scale to investigate electronic and optical applications of boron nitride materials [7–9]. However, the optical properties of BNNTs can also be tuned by doping. For example, BNNTs are doped with organic molecules in such a way that the absorption edge is red-shifted under a static transverse electric field [10]. Doping BNNTs with organic molecules not only changes the original electronic and optical properties, but also induces charge transfer. For example, deeply occupied molecular states can be observed in reactions of BNNT-encapsulated nucleophilic organic molecules [4].

Since BNNTs have a cavity large enough to encapsulate targets, many studies have used BNNTs as nanocapsules for drug delivery, encapsulating targeted therapeutic drugs into BNNTs to provide sustained release [5,11–17]. The chemical constitution of organic matter or biomolecules will also affect the physical and chemical properties of the whole

system; in particular, the change in the band gap energy difference is an important indicator [18]. This difference can be used to assess its potential as a chemical or biosensor [19]. The main force for the drug molecule + BNNT complex is the van der Waals force [11,14]. When drug molecules are encapsulated into and bound to BNNTs, they will change the polarity of the pristine BNNTs [17]. In the previous literature, quantum mechanical simulations were used to study the encapsulation, and it was believed that the stable state is the physical adsorption inside the nanotube [20,21].

As mentioned before, BNNTs have good processing properties, and, by doping metal atoms, the energy gap can be narrowed, the surface can be activated, and the reactivity can be improved [22–24]. Adding metal atoms in BNNTs can increase the adsorption force, which is used to increase the adsorption strength of drugs [22,25,26], improve the sensing response, and enhance the application as a chemical sensor [27–29]. Metal atoms commonly used to modify the properties of BNNTs include aluminum, iron, gallium, and others [30–33]. Although the mechanical properties of aluminum are relatively low, due to its low density and good formability, Al-doped materials are light in weight, corrosion-resistant, and have good mechanical properties [34]; Al-doped BNNT is also suitable as a drug carrier [35].

The geometry and properties of Al-doped BNNTs can be determined by weak electrostatic forces [36]. In addition to the van der Waals force of pristine BNNT, it is also subject to ionic interactions [22]. Al-doped BNNTs can have two types of atomic substitution, substitution on a boron atom or nitrogen atom. In the case of substituting boron atoms, aluminum atoms form Al-N bonds with surrounding nitrogen atoms, and the electron density distribution of Al-N bonds is similar to that of pristine B-N bonds [37].

Organophosphorus (OP) pesticides are known to be neurotoxic, and they enter the human body through various routes, posing threats to human health and animal survival [38–40]. If the degradability of OP pesticides is low, coupled with strong soil adsorption, it is easy to produce residues, and the burden on the environment is also great [41]. However, despite their environmental impact, OP pesticides are still used to control insects to increase yields [42–44].

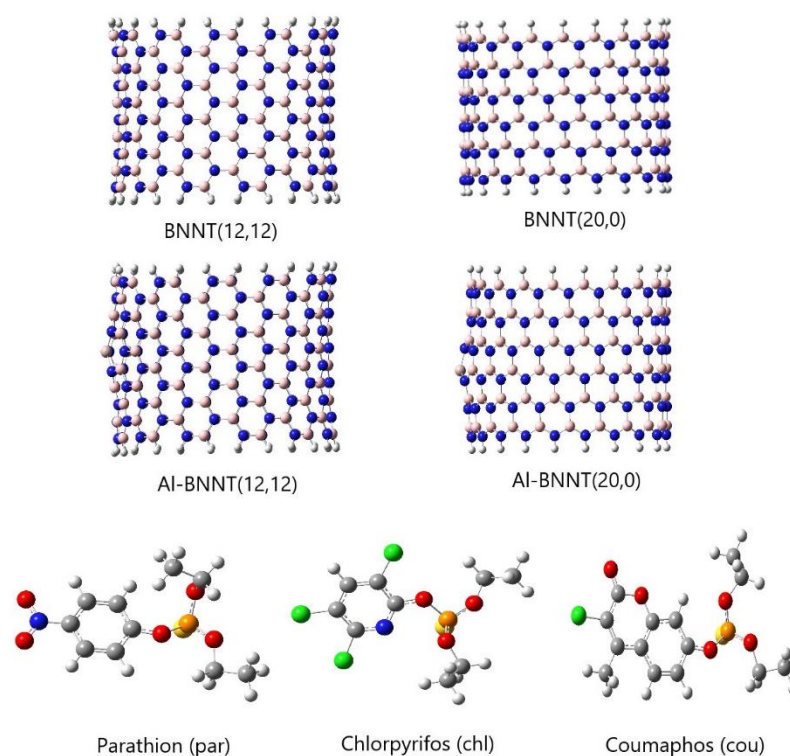
Controlled-release technology can realize the transfer of active ingredients from the reservoir to the target surface, and regulate and maintain the active ingredients at a predetermined concentration within a specific period of time [45]. The release kinetics of nano-encapsulated pesticides can be controlled, which can effectively enhance the permeability, stability, and solubility [46]. With efficient loading and controlled, targeted delivery, nano-encapsulated pesticides have received extensive attention internationally [47]. Nano-encapsulated pesticides can be used as intelligent pesticides with precise and controlled-release modes, which have the characteristics of light sensitivity, heat sensitivity, humidity sensitivity, and responses to soil pH and enzyme activity [48]. The previous literature also focused on the new applications of nanomaterials in bio-pesticides, nucleic acid pesticides, plant growth regulators, pheromones, and other agrochemicals [49]. Nanomaterials such as metal–organic frameworks, inorganic non-metallic materials, synthetic polymer materials, and natural polymer materials have been designed as pesticide carriers [50]. Encapsulants for agricultural controlled-release systems require environmentally friendly materials and manufacturing processes [51]. However, risk assessment analysis of nano-pesticides is the latest challenge to be overcome to accelerate the practical application of these novel nanomaterials by agricultural professionals [52].

We previously studied the adsorption of OP pesticides by BNNTs. The difference is that larger-sized BNNTs, armchair BNNT(12,12), and zigzag BNNT(20,0) are used in this study for the more stable adsorption of OP pesticides, namely encapsulation. Moreover, these two BNNTs are modified by replacing one boron atom with an aluminum atom to enhance the reactivity [26]. Four BNNTs encapsulating three OP pesticides with different polarities—parathion, chlorpyrifos, and coumaphos—are examined. Through reaction enthalpies, molecular electrostatic potentials, frontier molecular orbitals, and Hard and Soft Acid and Base (HSAB) descriptors derived from HOMO and LUMO values, the efficiency of

encapsulation and whether BNNT encapsulation has the property of sensing OP pesticides are discussed.

2. Computational Details

The Nanotube Modeler software (JCrystalSoft, 2018; Version 1.8) from <http://www.jcrystal.com/products/wincnt/> (accessed on 23 August 2021) was used to generate the XYZ coordinates of four types of boron nitride nanotube models, namely pristine armchair BNNT(12,12), pristine zigzag BNNT(20,0), Al-doped armchair BNNT(12,12), and Al-doped zigzag BNNT(20,0). Al-doped indicates that the boron site of BNNT is replaced by an Al atom. The four BNNT models with the edge atoms terminated by monohydrogen were used for the following calculations. The investigated organic pollutants included parathion (par), chlorpyrifos (chl), and coumaphos (cou) (Scheme 1).



Scheme 1. The four BNNT models (pristine armchair BNNT(12,12), pristine zigzag BNNT(20,0), Al-doped armchair BNNT(12,12), and Al-doped zigzag BNNT(20,0)) and the investigated organophosphorus pesticides (parathion (par), chlorpyrifos (chl), and coumaphos (cou)).

Geometry optimization was performed using the PM7 method in the MOPAC 2016 quantum chemistry software [53], available from <http://openmopac.net> (accessed on 15 July 2021). The solvent effect is implicitly treated by the conductor-like screening model (COSMO), which uses a dielectric constant of 78.4 for water [54]. All Density Functional Theory (DFT) calculations were performed by the Gaussian 16 software package [55]. The electronic properties were obtained using the M06-2X density functional method [56] and the 6-31G (d,p) basis set. The solvent effect of water is modeled by the polarizable continuum model using the integral equation formalism variant (IEF-PCM) [57]. The encapsulation energy can be defined as the following Equation (1):

$$E_{\text{enc}} = E(\text{OP}@(\text{Al-})\text{BNNT}) - E((\text{Al-})\text{BNNT}) - E(\text{OP}) \quad (1)$$

where $E(\text{OP}@(\text{Al-})\text{BNNT})$ is the total energy of the organophosphorus pesticide molecule (OP = par, chl and cou) encapsulated in (Al-doped) BNNT. $E((\text{Al-})\text{BNNT})$ and $E(\text{OP})$ are

the total energies of the (Al-doped) BNNT and the isolated organophosphorus pesticide molecule, respectively.

Chemical reactivity descriptors (GAP, I, A, μ , χ , η , S, ω) were calculated according to the highest occupied molecular orbital (HOMO) and the lowest unoccupied molecular orbital (LUMO) energies. The HOMO and LUMO energies are used to approximate ionization potential ($I = -\text{HOMO}$) and electron affinity ($A = -\text{LUMO}$), respectively [58]. The following HSAB descriptors can be calculated using the ionization potential (I) and electron affinity (A): the chemical potential ($\mu = -(I + A)/2$), electronegativity ($\chi = (I + A)/2 = -\mu$), chemical hardness ($\eta = (I - A)/2$), chemical softness ($S = 1/2\eta$), and electrophilicity index ($\omega = \mu^2/2\eta$) [59].

3. Results and Discussion

3.1. Encapsulation Energy

One characteristic of BN materials is that the B-N bond is a polar bond, due to the relatively large difference in electronegativity between B and N. The larger atomic partial charges bring out pronounced electrostatic interactions. The result of encapsulation energy is shown in Table 1, and it can be seen that without Al doping, the binding affinity of zigzag BNNT is greater than that of armchair BNNT to encapsulate parathion. The polarity of chlorpyrifos is relatively smaller than parathion, leading to the opposite result compared to parathion. This is because the polarity difference between zigzag BNNT and armchair BNNT is significantly large (zigzag > armchair). Doping with Al leads to the same situation. The phosphorothioate group is one of the active structures of OP pesticides. The nitro group of parathion and the oxygen atom on the coumarinyl group of coumaphos have a high negative charge, which facilitates the encapsulation.

Table 1. Encapsulation energy (calculated using Equation (1), in kcal/mol) of parathion (par), chlorpyrifos (chl), and coumaphos (cou) encapsulated by the nano-systems of BNNT(12,12), BNNT(20,0), Al-doped BNNT(12,12), and Al-doped BNNT(20,0).

			Encapsulation Energy (E_{enc}) (kcal/mol)
Armchair BNNT			
BNNT(12,12)	+par	BNNT(12,12) + par	−12.49
BNNT(12,12)	+chl	BNNT(12,12) + chl	−7.10
BNNT(12,12)	+cou	BNNT(12,12) + cou	−6.81
Zigzag BNNT			
BNNT(20,0)	+par	BNNT(20,0) + par	−12.92
BNNT(20,0)	+chl	BNNT(20,0) + chl	−5.63
BNNT(20,0)	+cou	BNNT(20,0) + cou	−11.72
Armchair BNNT			
Al-BNNT(12,12)	+par	Al-BNNT(12,12) + par	−12.81
Al-BNNT(12,12)	+chl	Al-BNNT(12,12) + chl	−8.17
Al-BNNT(12,12)	+cou	Al-BNNT(12,12) + cou	−12.96
Zigzag BNNT			
Al-BNNT(20,0)	+par	Al-BNNT(20,0) + par	−14.06
Al-BNNT(20,0)	+chl	Al-BNNT(20,0) + chl	−6.40
Al-BNNT(20,0)	+cou	Al-BNNT(20,0) + cou	−12.70

From the results summarized in Table 1, it can be seen that after Al doping, the encapsulation energy tends to decrease. Among them, Al-BNNT(20,0) + par has the lowest encapsulation energy. The order of encapsulation energy of zigzag BNNT(20,0) and Al-doped zigzag BNNT(20,0) with three organophosphorus pesticides is chlorpyrifos > coumaphos > parathion. This is the opposite order regarding the dipole moment and polarity for the three organophosphate pesticides (parathion > coumaphos > chlorpyrifos).

The phosphorothioate group is the core structure of parathion, coumaphos, and chlorpyrifos. The nitro group of parathion and the coumarin group of coumaphos have obvious ionic characteristics. For the chlorpyrifos structure, only the chlorine atom with

a small charge interacts with the BNNT tube wall. In addition, parathion has the largest conjugated system, so that the electrons will not be concentrated in a specific region, the repulsive force caused is weakened, and the system is relatively stable.

BNNT(12,12) + cou has the highest encapsulation energy of parathion and coumaphos among all BNNTs. This is because when cou is encapsulated into BNNT(12,12), the distance between the sulfur atom of the phosphorothioate group and the nearest boron atom is 3.20 Å, while that between the oxygen atom of the coumarin group and the nearest boron atom is 3.82 Å. Compared with the original structure of cou, shortening the distance between the ethyl group on the phosphorothioate group and the coumarin group caused obvious distortion and compression, and increased the energy barrier.

The Al-BNNT(20,0) + par system demonstrates the strongest encapsulation efficiency. The distances from the oxygen atom of the phosphorothioate group and the nitro groups to the nearest boron atom are 4.33 Å and 2.94 Å, respectively. DFT calculations using M06-2X/6-31G (d,p) were used to analyze the interactions and electronic properties of the systems. The result indicated that the value of the encapsulation energy of Al-BNNT(20,0) + par was the lowest in this work, and Al-BNNT(20,0) is suitable as a carrier for parathion.

3.2. Molecular Electrostatic Potential

The encapsulation of OP pesticide in BNNTs will cause charge redistribution, and the positive potential is concentrated at one end of the BNNT, indicating that the BNNT is an electron outflow system, and zigzag BNNT is more positive than armchair BNNT. The negative potential is mainly distributed in the high-electronegativity region of OP pesticide (Figures 1–3).

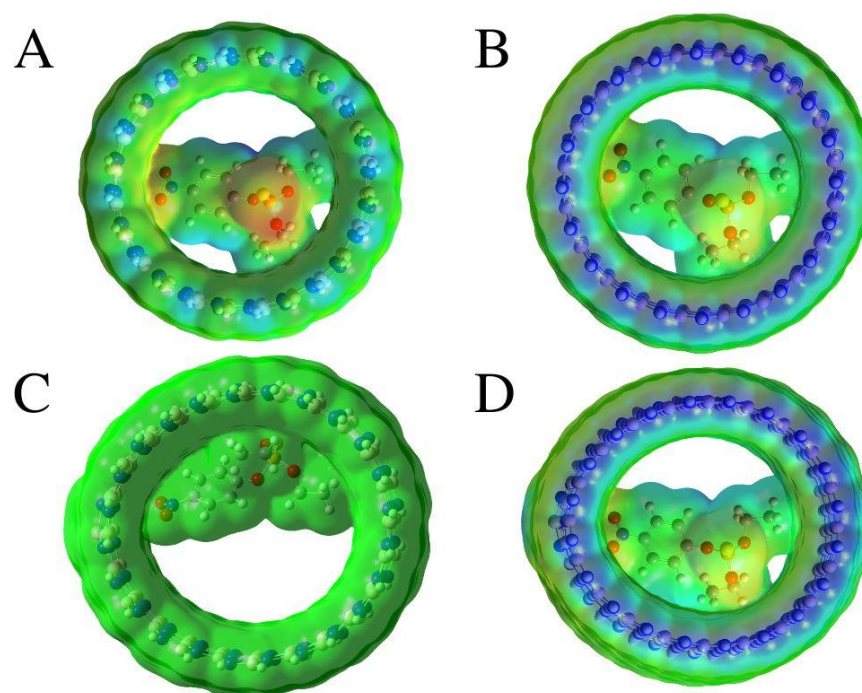


Figure 1. Electrostatic potentials of (A) BNNT(12,12) + par, (B) BNNT(20,0) + par, (C) Al-BNNT(12,12) + par, and (D) Al-BNNT(20,0) + par.

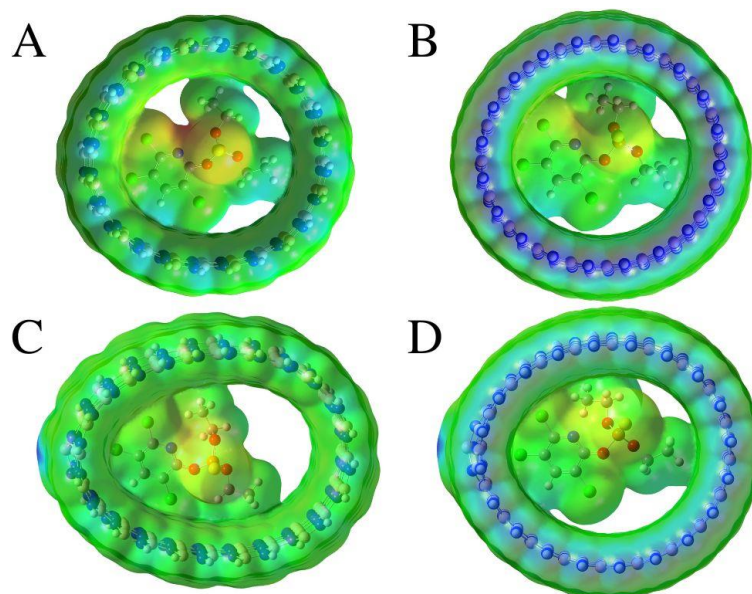


Figure 2. Electrostatic potentials of (A) BNNT(12,12) + chl, (B) BNNT(20,0) + chl, (C) Al-BNNT(12,12) + chl, and (D) Al-BNNT(20,0) + chl.

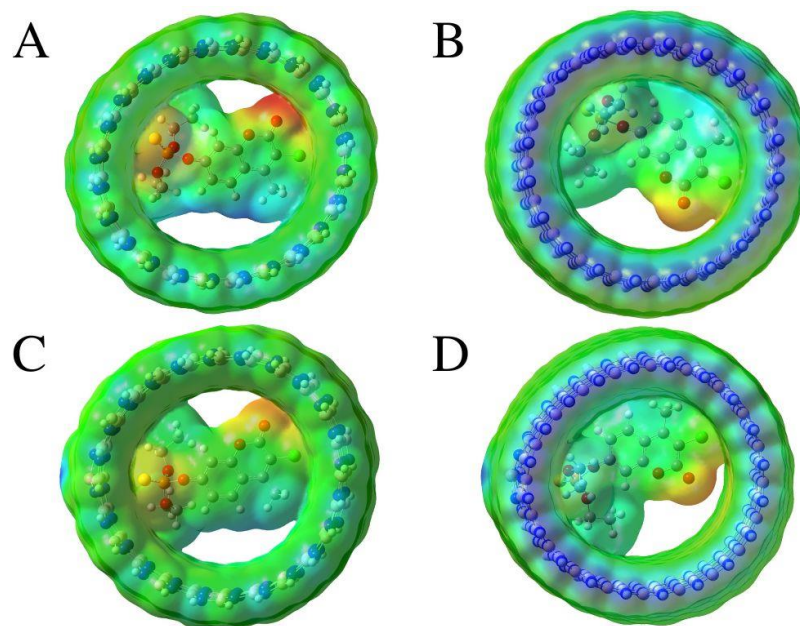


Figure 3. Electrostatic potentials of (A) BNNT(12,12) + cou, (B) BNNT(20,0) + cou, (C) Al-BNNT(12,12) + cou, and (D) Al-BNNT(20,0) + cou.

The phosphorothioate group is the core of the organophosphorus pesticide and also the location of the concentration of negative charges. In addition to phosphorothioate groups, negative charges are also concentrated on highly electronegative functional groups and atoms, such as the nitro group in parathion, the nitrogen atom of pyridine in chlorpyrifos and the oxygen atom of coumarin in coumaphos. These highly negative positions are the active sites of the reaction and contribute the main force of encapsulation. Especially for BNNT(12,12) + cou (Figure 3A), the oxygen atoms on the coumarinyl group are highly electronegative, showing a red-yellow color.

After Al doping, the position of the Al atom is a significant electron outflow, showing a dark blue color with a positive potential. It is worth mentioning that the OP pesticide

is green after the encapsulation of Al-BNNT(12,12) + par (Figure 1C), indicating that the polarization of the OP pesticide is less obvious in this case [20,21].

3.3. Hard and Soft Acid and Base (HSAB)

The HSAB descriptors are listed in Table 2. The energy gap between HOMO and LUMO ($GAP = LUMO - HOMO$) represents the energy difference that needs to be overcome for electron transfer. The larger the GAP difference, the more difficult it is for the electrons of this molecule to transition. Compounds with larger energy gaps have higher chemical hardness. The GAP values of armchair BNNT are larger than those of zigzag BNNT, and that of pristine BNNT is larger than that of Al-doped BNNT, which has the same order as the ionization energy. Al doping contributes to narrowing the GAP [23], which has a smaller energy to overcome for electron transfer than pristine BNNT. When OP pesticides are encapsulated into BNNTs, the GAP becomes smaller. The reaction of OP pesticides with BNNT(12,12) has the largest GAP change; moreover, the GAP of BNNT(12,12) + cou has the largest change, so that BNNT(12,12) is the most suitable as a chemical sensor [19].

Table 2. The HSAB descriptors in the present study ^a.

	GAP (eV)	I (eV)	A (eV)	χ (eV)	η (eV)	μ (eV)	S (eV ⁻¹)	ω (eV)
par	6.825	8.447	1.622	5.034	3.412	-5.034	0.147	3.714
chl	7.443	8.051	0.608	4.330	3.721	-4.330	0.134	2.519
cou	6.338	7.542	1.204	4.373	3.169	-4.373	0.158	3.017
BNNT(12,12)	8.793	8.026	-0.767	3.630	4.396	-3.630	0.114	1.498
BNNT(20,0)	8.273	7.868	-0.405	3.732	4.137	-3.732	0.121	1.683
BNNT(12,12) + par	6.398	8.009	1.611	4.810	3.199	-4.810	0.156	3.616
BNNT(12,12) + chl	7.316	8.028	0.712	4.370	3.658	-4.370	0.137	2.611
BNNT(12,12) + cou	6.373	7.707	1.334	4.520	3.187	-4.520	0.157	3.206
BNNT(20,0) + par	6.230	7.844	1.614	4.729	3.115	-4.729	0.161	3.590
BNNT(20,0) + chl	7.222	7.866	0.644	4.255	3.611	-4.255	0.138	2.507
BNNT(20,0) + cou	6.344	7.666	1.322	4.494	3.172	-4.494	0.158	3.184
Al-BNNT(12,12)	7.686	8.017	0.330	4.174	3.843	-4.174	0.130	2.266
Al-BNNT(20,0)	7.603	7.856	0.253	4.054	3.802	-4.054	0.132	2.162
Al-BNNT(12,12) + par	6.391	7.996	1.605	4.801	3.196	-4.801	0.156	3.606
Al-BNNT(12,12) + chl	7.234	8.010	0.776	4.393	3.617	-4.393	0.138	2.668
Al-BNNT(12,12) + cou	6.357	7.696	1.339	4.518	3.179	-4.518	0.157	3.210
Al-BNNT(20,0) + par	6.154	7.834	1.679	4.756	3.077	-4.756	0.162	3.676
Al-BNNT(20,0) + chl	7.256	7.847	0.591	4.219	3.628	-4.219	0.138	2.453
Al-BNNT(20,0) + cou	6.309	7.614	1.305	4.460	3.154	-4.460	0.159	3.152

^a Energy gap: $GAP =$ the lowest unoccupied molecular orbital (LUMO) energy—the highest occupied molecular orbital (HOMO) energy; ionization potential: $I = -HOMO$; electron affinity: $A = -LUMO$ [58]; chemical potential: $\mu = -(I + A)/2$; electronegativity: $\chi = (I + A)/2 = -\mu$; chemical hardness: $\eta = (I - A)/2$; chemical softness: $S = 1/2\eta$; electrophilicity index: $\omega = \mu^2/2\eta$ [59].

HOMO is the highest molecular orbital occupied by electrons. The larger the energy, the stronger the ability to donate electrons. The negative value of the HOMO is ionization energy ($I = -HOMO$), which is the minimum energy required to remove one of the electrons from an atom or molecule. The order is par > chl > cou, and armchair BNNT is greater than zigzag BNNT and pristine BNNT is greater than Al-doped BNNT. When parathion is adsorbed in the nano-system, the ionization energy becomes smaller, and the ionization energy of BNNT(12,12) changes less than that of BNNT(20,0). Coumaphos has the largest HOMO value, which means that it has the smallest ionization energy and has the strongest ability to donate electrons.

LUMO is the lowest unoccupied molecular orbital. The smaller the energy, the stronger the ability to accept electrons. The negative value of the LUMO is electron affinity ($A = -LUMO$), which is the energy released when the system accepts an electron. The order is par > cou > chl, and Al-doped BNNTs are greater than pristine BNNTs. When encapsulating coumaphos, the electron affinity becomes larger, and the change in the electron

affinity of zigzag BNNTs is smaller than that of armchair BNNTs. When the coumaphos is encapsulated by BNNT, the electron affinity becomes larger.

The electronegativity ($\chi = (I + A)/2 = -\mu$) means that electrons migrate to the system with higher electronegativity. The order is par > cou > chl. Because parathion has nitrogen and oxygen atoms, which possess high electronegativity, this leads to parathion having the greatest electronegativity. Aluminum atoms possess less electronegativity than boron and nitrogen atoms. After Al doping, the electron affinity and electronegativity increase [26], and the electronegativity difference with OP pesticides decreases, which will weaken the interaction between the two and reduce the encapsulation energy. It shows that Al-doped BNNT has the potential to be a carrier of OP pesticides [28]. Compared with chlorpyrifos and coumaphos, parathion has the largest ionization energy, electron affinity, and electronegativity, because it has the largest conjugated system, making the electron distribution delocalized and increasing the relative stability of the system.

For the chemical potential ($\mu = -(I + A)/2$), the order is opposite to that of electronegativity, due to the chemical potential being the negative value of electronegativity. Those with higher chemical potential tend to act as electron donors, providing electrons to those with lower chemical potential. BNNTs have higher chemical potential than OP pesticides; when OP pesticides react with BNNTs, OP pesticides tend to act as electron acceptors, and BNNTs tend to act as electron donors.

The chemical hardness ($\eta = (I - A)/2$) represents the stability of the entire system. The greater the chemical hardness, the more difficult it is for the charge to transfer, which reduces the polarization and improves the stability of the system. The order is chl > par > cou. The chemical hardness of zigzag BNNT is smaller than that of armchair BNNT, and the phenomenon of polarization will be more obvious during the reaction. This can explain why the blue part of the zigzag BNNT in the electrostatic potential diagram is deeper than that of the armchair BNNT. During encapsulation, the chemical hardness of the four types of BNNTs becomes smaller, and the change in the chemical hardness of BNNT(12,12) declines the most.

The chemical softness ($S = 1/2\eta$) has opposite characteristics to chemical hardness: the higher the chemical softness, the easier it is to be polarized, so that the order is the opposite of chemical hardness. The chemical softness of zigzag BNNTs is larger than that of armchair BNNTs, and Al-doped BNNTs have larger values than pristine BNNTs, which means that Al-BNNT(20,0) is more easily polarized and therefore has higher reactivity. When OP pesticides are encapsulated in the nano-system, the chemical softness becomes larger, and the chemical softness of BNNT(12,12) increases the most.

Because soft acids form strong bonds with soft bases, and hard acids form strong bonds with hard bases, Al-BNNT(20,0) + cou is the softest OP pesticide encapsulated into the softest BNNT, and BNNT(12,12) + chl is the hardest OP pesticide encapsulated into the hardest BNNT. Coumaphos has the least chemical hardness and reacts with BNNT(12,12), which has high chemical potential and low polarity, leading to higher encapsulation energy. Chlorpyrifos can react with BNNT to obtain higher chemical hardness. Moreover, BNNT(12,12) + chl is the complex with the largest GAP and chemical hardness in the reaction between OP pesticides and BNNTs, which means that it is difficult to excite electrons during the transition process and the molecular stability is high.

For the electrophilicity index ($\omega = \mu^2/2\eta$), the larger the value, the easier it is to accept electrons. Parathion has a nitro group, which leads to it having the largest electrophilicity index. The electrophilicity index of Al-doped BNNTs is much larger than that of pristine BNNTs, indicating that the degree of electron acceptance is increased. Furthermore, Al-BNNT(12,12) has the largest electrophilicity index among the four types of BNNTs. OP pesticides have a higher electrophilicity index and play the role of an electron acceptor in the system, among which parathion has the largest electrophilicity index. The larger the electrophilicity index, the more suitable it is as an electrophile in chemical reactions.

3.4. Frontier Molecular Orbital (FMO)

When parathion or chlorpyrifos is encapsulated into BNNTs, the orbital lobes in the HOMO diagram are mainly distributed on the BNNTs (Figures 4 and 5). Due to electronegativity, the orbital lobes are located on the nitrogen atoms and N-B bonds of BNNTs. The HOMO orbital lobes of BNNT(12,12) + chl are light green and uniformly distributed in the BNNT (Figure 5A). In particular, for Al-BNNT(12,12) + chl (Figure 5C), the HOMO is slightly distributed on the orbital lobes of the trichloropyridyl group. This is because when chl is encapsulated by Al-BNNT(12,12), the optimized geometry of BNNT is obviously deformed, allowing the OP to cling to the inner wall of the BNNT.

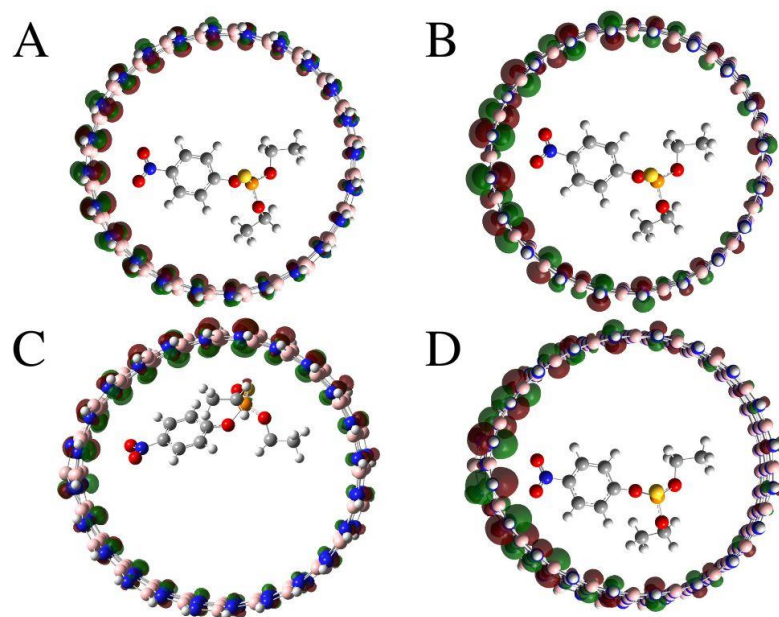


Figure 4. The HOMO diagrams of (A) BNNT(12,12) + par, (B) BNNT(20,0) + par, (C) Al-BNNT(12,12) + par, and (D) Al-BNNT(20,0) + par.

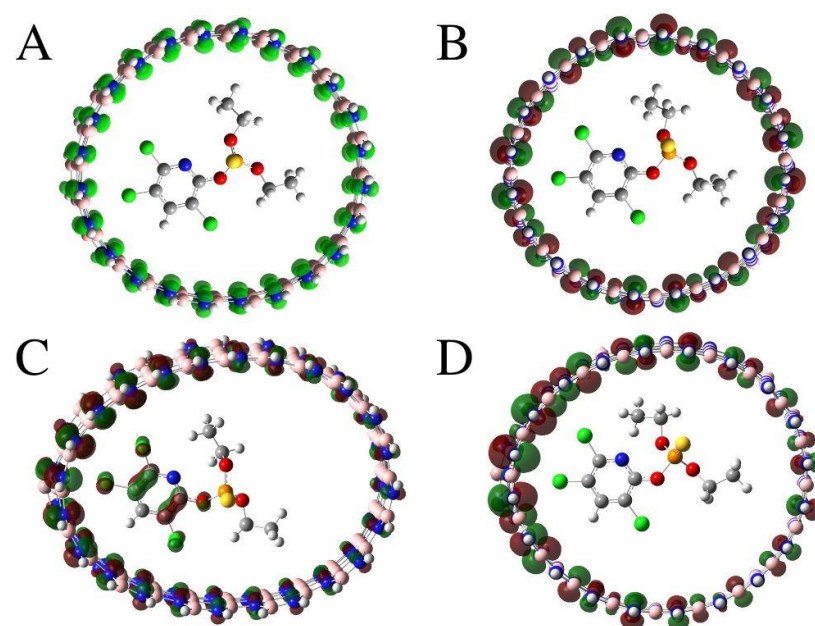


Figure 5. The HOMO diagrams of (A) BNNT(12,12) + chl, (B) BNNT(20,0) + chl, (C) Al-BNNT(12,12) + chl, and (D) Al-BNNT(20,0) + chl.

However, unlike parathion and chlorpyrifos, the orbital lobes in the HOMO diagram are concentrated on the coumarinyl group, oxygen atom, and chlorine atom of coumaphos (Figure 6). This may be due to the fact that coumaphos has the highest HOMO value (HOMO = -7.542 eV) among the three OP pesticides, which leads to the electron-occupied orbital dominance of the BNNT + cou system. As for the LUMO diagram, the results given are similar (Figures 7–9). The orbital lobes are concentrated on the nitrophenyl group of par, the trichloropyridyl group of chl, and the coumarinyl group of the cou pesticide. As a result, OP pesticides are electrophiles, while BNNTs are nucleophiles.

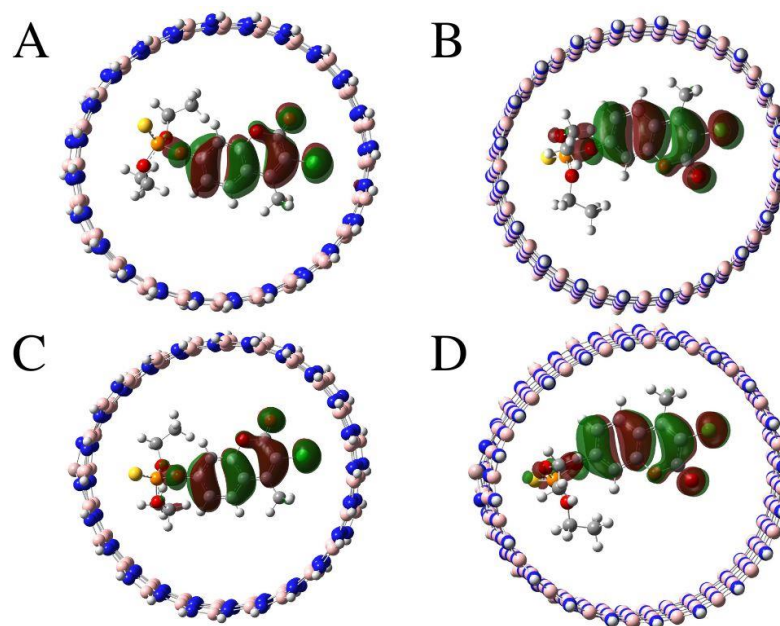


Figure 6. The HOMO diagrams of (A) BNNT(12,12) + cou, (B) BNNT(20,0) + cou, (C) Al-BNNT(12,12) + cou, and (D) Al-BNNT(20,0) + cou.

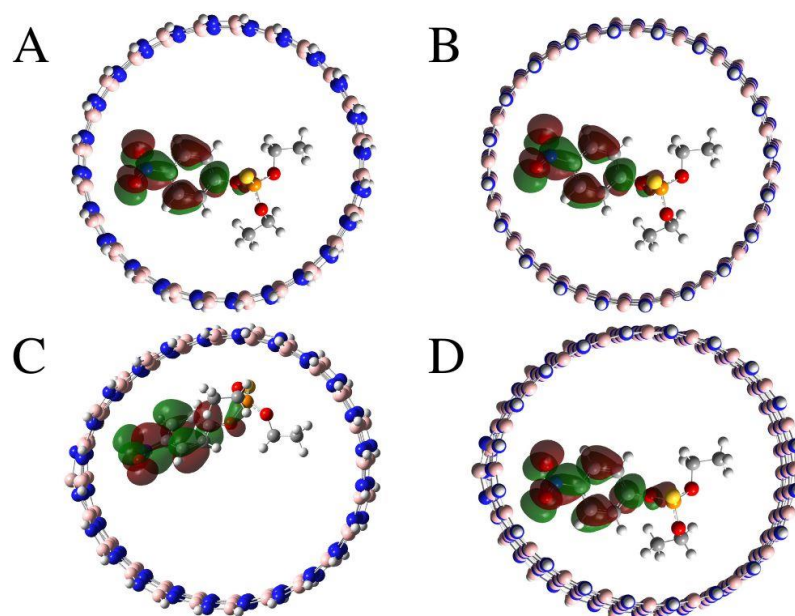


Figure 7. The LUMO diagrams of (A) BNNT(12,12) + par, (B) BNNT(20,0) + par, (C) Al-BNNT(12,12) + par, and (D) Al-BNNT(20,0) + par.

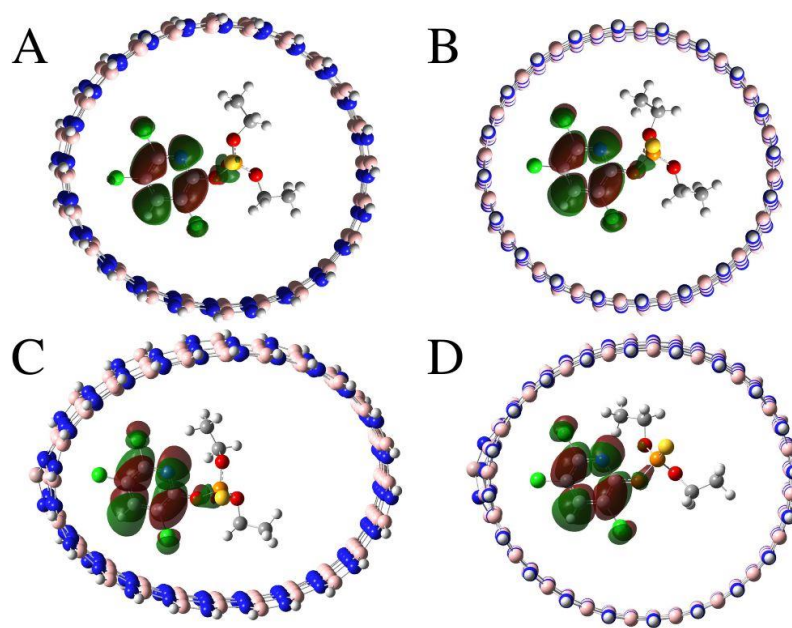


Figure 8. The LUMO diagrams of (A) BNNT(12,12) + chl, (B) BNNT(20,0) + chl, (C) Al-BNNT(12,12) + chl, and (D) Al-BNNT(20,0) + chl.

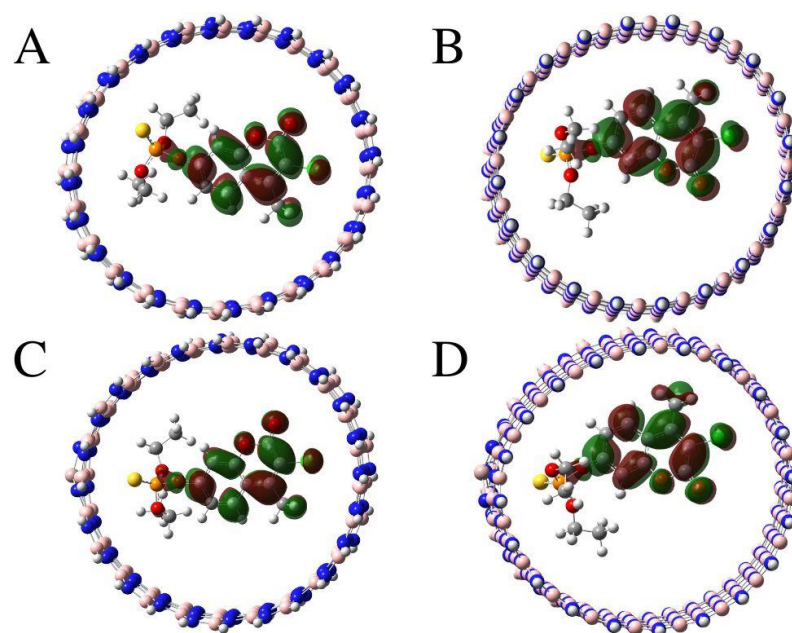


Figure 9. The LUMO diagrams of (A) BNNT(12,12) + cou, (B) BNNT(20,0) + cou, (C) Al-BNNT(12,12) + cou, and (D) Al-BNNT(20,0) + cou.

4. Conclusions

We investigated four BNNTs and their interactions with three OP pesticides and found that the Al-doped zigzag BNNT(20,0) + parathion system has the highest encapsulation efficiency. Al doping helps to decrease the encapsulation energy. It enhances the reactivity of the OP pesticides involved in encapsulation. Armchair BNNT(12,12) exhibits significant energy gap changes with three OP pesticides, among which armchair BNNT(12,12) + coumaphos has the largest energy gap change.

Author Contributions: Conceptualization, R.-L.W. and C.M.C.; methodology, R.-L.W. and C.M.C.; software, R.-L.W.; validation, C.M.C.; formal analysis, R.-L.W. and C.M.C.; investigation, R.-L.W.; resources, C.M.C.; data curation, R.-L.W.; writing—original draft preparation, R.-L.W.; writing—review and editing, C.M.C.; visualization, R.-L.W. and C.M.C.; supervision, C.M.C.; project administration, C.M.C.; funding acquisition, C.M.C. All authors have read and agreed to the published version of the manuscript.

Funding: This research was funded by the National Science Council of Taiwan, Republic of China, under grant number MOST 111-2321-B-005-004.

Data Availability Statement: Not applicable.

Acknowledgments: The authors thank the National Science Council of Taiwan, Republic of China, MOST 111-2321-B-005-004, for providing financial support. Computer time was provided by the National Center for High-Performance Computing.

Conflicts of Interest: The authors declare no conflict of interest.

References

1. Lin, Y.; Connell, J.W. Advances in 2D boron nitride nanostructures: Nanosheets, nanoribbons, nanomeshes, and hybrids with graphene. *Nanoscale* **2012**, *4*, 6908–6939. [[CrossRef](#)] [[PubMed](#)]
2. Blase, X.; Rubio, A.; Louie, S.G.; Cohen, M.L. Stability and band-gap constancy of boron-nitride nanotubes. *Europhys. Lett.* **1994**, *28*, 335–340. [[CrossRef](#)]
3. Shao, P.; Kuang, X.-Y.; Ding, L.-P.; Yang, J.; Zhong, M.-M. Can CO₂ molecule adsorb effectively on Al-doped boron nitride single walled nanotube? *Appl. Surf. Sci.* **2013**, *285*, 350–356. [[CrossRef](#)]
4. He, W.; Li, Z.; Yang, J.; Hou, J.G. A first principles study on organic molecule encapsulated boron nitride nanotubes. *J. Chem. Phys.* **2008**, *128*, 164701. [[CrossRef](#)] [[PubMed](#)]
5. Zarghami Dehaghani, M.; Bagheri, B.; Nasiriasayesh, A.; Mashhadzadeh, A.H.; Zarrintaj, P.; Rabiee, N.; Bagherzadeh, M.; Habibzadeh, S.; Abida, O.; Saeb, M.R.; et al. Insight into the Self-Insertion of a Protein Inside the Boron Nitride Nanotube. *ACS Omega* **2020**, *5*, 32051–32058. [[CrossRef](#)]
6. Weng, Q.; Wang, X.; Wang, X.; Bando, Y.; Golberg, D. Functionalized hexagonal boron nitride nanomaterials: Emerging properties and applications. *Chem. Soc. Rev.* **2016**, *45*, 3989–4012. [[CrossRef](#)]
7. Jonuarti, R. The Ultra-Small Armchair Boron Nitride Nanotubes Study Using a Density Functional Theory Method. *J. Phys. Conf. Ser.* **2020**, *1428*, 012005. [[CrossRef](#)]
8. Zhang, Z.; Guo, W.; Dai, Y. Freestanding (3,0) boron nitride nanotube: Expected to be stable well over room temperature. *Appl. Phys. Lett.* **2008**, *93*, 22310. [[CrossRef](#)]
9. Zhang, J.-M.; Wang, S.-F.; Du, X.-J.; Xu, K.-W.; Ji, V. Comparison of Electronic and Magnetic Properties of Fe, Co, and Ni Nanowires Encapsulated in Boron Nitride Nanotubes. *J. Phys. Chem. C* **2009**, *113*, 41. [[CrossRef](#)]
10. He, W.; Li, Z.; Yang, J.; Hou, J.G. Electronic structures of organic molecule encapsulated BN nanotubes under transverse electric field. *J. Chem. Phys.* **2008**, *129*, 024710. [[CrossRef](#)]
11. Mirhaji, E.; Afshar, M.; Rezvani, S.; Yoosefian, M. Boron nitride nanotubes as a nanotransporter for anti-cancer docetaxel drug in water/ethanol solution. *J. Mol. Liq.* **2018**, *271*, 151–156. [[CrossRef](#)]
12. Datz, D.; Németh, G.; Walker, K.E.; Rance, G.A.; Pekker, Á.; Khlobystov, A.N.; Kamarás, K. Polaritonic Enhancement of Near-Field Scattering of Small Molecules Encapsulated in Boron Nitride Nanotubes: Chemical Reactions in Confined Spaces. *ACS Appl. Nano Mater.* **2021**, *4*, 4335–4339. [[CrossRef](#)]
13. Zarghami Dehaghani, M.; Bagheri, B.; Yousefi, F.; Nasiriasayesh, A.; Hamed Mashhadzadeh, A.; Zarrintaj, P.; Rabiee, N.; Bagherzadeh, M.; Fierro, V.; Celzard, A.; et al. Boron Nitride Nanotube as an Antimicrobial Peptide Carrier: A Theoretical Insight. *Int. J. Nanomed.* **2021**, *16*, 1837–1847. [[CrossRef](#)] [[PubMed](#)]
14. Zarghami Dehaghani, M.; Yousefi, F.; Sajadi, S.M.; Tajammal Munir, M.; Abida, O.; Habibzadeh, S.; Mashhadzadeh, A.H.; Rabiee, N.; Mostafavi, E.; Saeb, M.R. Theoretical Encapsulation of Fluorouracil (5-FU) Anti-Cancer Chemotherapy Drug into Carbon Nanotubes (CNT) and Boron Nitride Nanotubes (BNNT). *Molecules* **2021**, *26*, 4920. [[CrossRef](#)]
15. Roosta, S.; Nikkha, S.J.; Sabzali, M.; Hashemianzadeh, S.M. Molecular dynamics simulation study of boron-nitride nanotubes as a drug carrier: From encapsulation to releasing. *RSC Adv.* **2016**, *6*, 9344–9351. [[CrossRef](#)]
16. El Khalifi, M.; Bentin, J.; Duverger, E.; Gharbi, T.; Boulahdour, H.; Picaud, F. Encapsulation capacity and natural payload delivery of an anticancer drug from boron nitride nanotube. *Phys. Chem. Chem. Phys.* **2016**, *18*, 24994–25001. [[CrossRef](#)]
17. Samanta, P.N.; Das, K.K. 5-Aminolevulinic acid functionalized boron-nitride and carbon nanotubes as drug delivery vehicles for skin anticancer drugs: A theoretical study. *RSC Adv.* **2016**, *6*, 92547–92559. [[CrossRef](#)]
18. Feng, L.-y.; Liu, Y.-j.; Zhao, J.-x.; Ding, Y.-h. Theoretical Study on the Encapsulation of Li Atoms inside Boron Nitride Nanotubes: Physical Properties and Catalytic Reactivity for the Oxygen Reduction Reaction. *J. Phys. Chem. C* **2014**, *118*, 30325–30332. [[CrossRef](#)]

19. Saikia, N.; Taha, M.; Pandey, R. Molecular insights on the dynamic stability of peptide nucleic acid functionalized carbon and boron nitride nanotubes. *Phys. Chem. Chem. Phys.* **2021**, *23*, 219–228. [[CrossRef](#)]
20. El Khalifi, M.; Duverger, E.; Gharbi, T.; Boulahdour, H.; Picaud, F. Theoretical demonstration of the potentiality of boron nitride nanotubes to encapsulate anticancer molecule. *Phys. Chem. Chem. Phys.* **2015**, *17*, 30057–30064. [[CrossRef](#)]
21. El Khalifi, M.; Duverger, E.; Gharbi, T.; Boulahdour, H.; Picaud, F. Theoretical use of boron nitride nanotubes as a perfect container for anticancer molecules. *Anal. Methods* **2016**, *8*, 1367–1372. [[CrossRef](#)]
22. Mohammadi, M.D.; Abdullah, H.Y.; Biskos, G.; Bhowmick, S. Effect of Al- and Ga-doping on the adsorption of H₂SiCl₂ onto the outer surface of boron nitride nanotube: A DFT study. *Comptes Rendus. Chim.* **2021**, *24*, 291–304. [[CrossRef](#)]
23. Tavangar, Z.; Hamadianian, M.; Basharnavaz, H. Studying the effects of the configuration of doped Al atoms on the conductive properties of boron nitride nanotube using density functional theory. *Chem. Phys. Lett.* **2017**, *669*, 29–37. [[CrossRef](#)]
24. Soltani, A.; Moradi, A.V.; Bahari, M.; Masoodi, A.; Shojaee, S. Computational investigation of the electronic and structural properties of CN radical on the pristine and Al-doped (6, 0) BN nanotubes. *Phys. B Condens. Matter* **2013**, *430*, 20–26. [[CrossRef](#)]
25. Mohammadi, M.D.; Abdullah, H.Y. Weak intermolecular interactions of cysteine on BNNT, BNAINNT and BC2NNT: A DFT investigation. *Bull. Mater. Sci.* **2022**, *45*, 33. [[CrossRef](#)]
26. Peyab, R.; Hosseini, S.; Esrafil, M.D. Al- and Ga-embedded boron nitride nanotubes as effective nanocarriers for delivery of rizatriptan. *J. Mol. Liq.* **2022**, *361*, 119662. [[CrossRef](#)]
27. Zhang, Y.Q.; Liu, Y.J.; Liu, Y.L.; Zhao, J.X. Boosting sensitivity of boron nitride nanotube (BNNT) to nitrogen dioxide by Fe encapsulation. *J. Mol. Graph. Model.* **2014**, *51*, 1–6. [[CrossRef](#)]
28. Doust Mohammadi, M.; Abdullah, H.Y.; Kalamse, V.; Chaudhari, A. Interaction of Fluorouracil drug with boron nitride nanotube, Al doped boron nitride nanotube and BC₂N nanotube. *Comput. Theor. Chem.* **2022**, *1212*, 113699. [[CrossRef](#)]
29. Jasim, S.A.; Al-Gazally, M.E.; Opulencia, M.J.C.; Kadhim, M.M.; Mahdi, A.B.; Hammid, A.T.; Ebadi, A.G. Toxic hydrazoic acid vapor detection and adsorption by different metal-decorated BN nanotubes: A first-principles study. *Comput. Theor. Chem.* **2022**, *1212*, 113721. [[CrossRef](#)]
30. Farmanzadeh, D.; Rezaiejad, H. DFT Study of Adsorption of Diazinon, Hinosan, Chlorpyrifos and Parathion Pesticides on the Surface of B₃₆N₃₆ Nanocage and Its Fe Doped Derivatives as New Adsorbents. *Acta Phys.-Chim. Sin.* **2016**, *32*, 1191–1198. [[CrossRef](#)]
31. Javan, M.B.; Soltani, A.; Ghasemi, A.S.; Lemeski, E.T.; Gholami, N.; Balakheyli, H. Ga-doped and antisite double defects enhance the sensitivity of boron nitride nanotubes towards Soman and Chlorosoman. *Appl. Surf. Sci.* **2017**, *411*, 1–10. [[CrossRef](#)]
32. Nemati-Kande, E.; Karimian, R.; Goodarzi, V.; Ghazizadeh, E. Feasibility of pristine, Al-doped and Ga-doped Boron Nitride nanotubes for detecting SF₄ gas: A DFT, NBO and QTAIM investigation. *Appl. Surf. Sci.* **2020**, *510*, 145490. [[CrossRef](#)]
33. Doust Mohammadi, M.; Abdullah, H.Y. Vinyl chloride adsorption onto the surface of pristine, Al-, and Ga-doped boron nitride nanotube: A DFT study. *Solid. State Commun.* **2021**, *337*, 114440. [[CrossRef](#)]
34. Sedigh, P.; Zare, A.; Montazeri, A. Evolution in aluminum applications by numerically-designed high strength boron-nitride/Al nanocomposites. *Comput. Mater. Sci.* **2020**, *171*, 109227. [[CrossRef](#)]
35. Shakerzadeh, E.; Noorizadeh, S. A first principles study of pristine and Al-doped boron nitride nanotubes interacting with platinum-based anticancer drugs. *Phys. E Low-Dimens. Syst. Nanostruct.* **2014**, *57*, 47–55. [[CrossRef](#)]
36. Azizi, K.; Salabat, K.; Seif, A. Methane storage on aluminum-doped single wall BNNTs. *Appl. Surf. Sci.* **2014**, *309*, 54–61. [[CrossRef](#)]
37. Rohmann, C.; Yamakov, V.I.; Park, C.; Fay, C.; Hankel, M.; Searles, D.J. Interaction of Boron Nitride Nanotubes with Aluminium: A Computational Study. *J. Phys. Chem. C Nanomater. Interfaces* **2018**, *122*, 15226–15240. [[CrossRef](#)]
38. Sen, S.; Roy, A.; Sanyal, A.; Devi, P.S. A nonenzymatic reduced graphene oxide-based nanosensor for parathion. *Beilstein J. Nanotechnol.* **2022**, *13*, 730–744. [[CrossRef](#)]
39. Maggio, S.A.; Janney, P.K.; Jenkins, J.J. Neurotoxicity of chlorpyrifos and chlorpyrifos-oxon to *Daphnia magna*. *Chemosphere* **2021**, *276*, 130120. [[CrossRef](#)]
40. Kumar, S.; Sharma, A.K.; Kumar, B.; Shakya, M.; Patel, J.A.; Kumar, B.; Bisht, N.; Chigure, G.M.; Singh, K.; Kumar, R.; et al. Characterization of deltamethrin, cypermethrin, coumaphos and ivermectin resistance in populations of *Rhipicephalus microplus* in India and efficacy of an antitick natural formulation prepared from *Ageratum conyzoides*. *Ticks Tick. Borne Dis.* **2021**, *12*, 101818. [[CrossRef](#)]
41. Weerathunge, P.; Behera, B.K.; Zihara, S.; Singh, M.; Prasad, S.N.; Hashmi, S.; Mariathomas, P.R.D.; Bansal, V.; Ramanathan, R. Dynamic interactions between peroxidase-mimic silver NanoZymes and chlorpyrifos-specific aptamers enable highly-specific pesticide sensing in river water. *Anal. Chim. Acta* **2019**, *1083*, 157–165. [[CrossRef](#)] [[PubMed](#)]
42. Lee, C.L.; Chang, C.M. Quantum Chemical Approach to the Adsorption of Chlorpyrifos and Fenitrothion on the Carbon-Doped Boron Nitride Nanotube Decorated with Tetrapeptide. *Crystals* **2022**, *12*, 1285. [[CrossRef](#)]
43. Huang, S.G.; Wu, Y.; Hu, J.P.; Liu, M.H. Density Functional Theory Calculation and Raman Spectroscopy Studies of Organophosphorus Pesticides. *Spectrosc. Spectr. Anal.* **2017**, *37*, 135–140.
44. Caetano, M.S.; Ramalho, T.C.; Botrel, D.F.; da Cunha, E.F.F.; de Mello, W.C. Understanding the inactivation process of organophosphorus herbicides: A DFT study of glyphosate metallic complexes with Zn²⁺, Ca²⁺, Mg²⁺, Cu²⁺, Co³⁺, Fe³⁺, Cr³⁺, and Al³⁺. *Int. J. Quantum Chem.* **2012**, *112*, 2752–2762. [[CrossRef](#)]

45. Li, N.; Sun, C.; Jiang, J.; Wang, A.; Wang, C.; Shen, Y.; Huang, B.; An, C.; Cui, B.; Zhao, X.; et al. Advances in Controlled-Release Pesticide Formulations with Improved Efficacy and Targetability. *J. Agric. Food Chem.* **2021**, *69*, 12579–12597. [[CrossRef](#)]
46. Kumar, S.; Nehra, M.; Dilbaghi, N.; Marrazza, G.; Hassan, A.A.; Kim, K.-H. Nano-based smart pesticide formulations: Emerging opportunities for agriculture. *J. Control. Release* **2019**, *294*, 131–153. [[CrossRef](#)]
47. Singh, G.; Ramadass, K.; Sooriyakumar, P.; Hettithanthri, O.; Vithange, M.; Bolan, N.; Tavakkoli, E.; Van Zwieten, L.; Vinu, A. Nanoporous materials for pesticide formulation and delivery in the agricultural sector. *J. Control. Release* **2022**, *343*, 187–206. [[CrossRef](#)] [[PubMed](#)]
48. Huang, B.; Chen, F.; Shen, Y.; Qian, K.; Wang, Y.; Sun, C.; Zhao, X.; Cui, B.; Gao, F.; Zeng, Z.; et al. Advances in Targeted Pesticides with Environmentally Responsive Controlled Release by Nanotechnology. *Nanomaterials* **2018**, *8*, 102. [[CrossRef](#)]
49. An, C.; Sun, C.; Li, N.; Huang, B.; Jiang, J.; Shen, Y.; Wang, C.; Zhao, X.; Cui, B.; Wang, C.; et al. Nanomaterials and nanotechnology for the delivery of agrochemicals: Strategies towards sustainable agriculture. *J. Nanobiotechnol.* **2022**, *20*, 11. [[CrossRef](#)]
50. Tao, R.; You, C.; Qu, Q.; Zhang, X.; Deng, Y.; Ma, W.; Huang, C. Recent advances in the design of controlled- and sustained-release micro/nanocarriers of pesticide. *Environ. Sci. Nano* **2023**, *10*, 351–371. [[CrossRef](#)]
51. Lee, P.; Lin, X.; Khan, F.; Bennett, A.E.; Winter, J.O. Translating controlled release systems from biomedicine to agriculture. *Front. Biomater. Sci.* **2022**, *1*, 1011877. [[CrossRef](#)]
52. Villaverde, J.J.; Sevilla-Morán, B.; López-Goti, C.; Alonso-Prados, J.L.; Sandín-España, P. Considerations of nano-QSAR/QSPR models for nanopesticide risk assessment within the European legislative framework. *Sci. Total. Environ.* **2018**, *634*, 1530–1539. [[CrossRef](#)]
53. Stewart, J.J. Optimization of parameters for semiempirical methods VI: More modifications to the NDDO approximations and re-optimization of parameters. *J. Mol. Model.* **2013**, *19*, 1–32. [[CrossRef](#)]
54. Klamt, A.; Schüürmann, G. COSMO: A new approach to dielectric screening in solvents with explicit expressions for the screening energy and its gradient. *J. Chem. Soc. Perkin Trans.* **1993**, *2*, 799–805. [[CrossRef](#)]
55. Frisch, M.e.; Trucks, G.; Schlegel, H.B.; Scuseria, G.; Robb, M.; Cheeseman, J.; Scalmani, G.; Barone, V.; Petersson, G.; Nakatsuji, H. *Gaussian 16 Rev. C.01*; Gaussian, Inc.: Wallingford, CT, USA, 2016.
56. Zhao, Y.; Truhlar, D.G. The M06 suite of density functionals for main group thermochemistry, thermochemical kinetics, noncovalent interactions, excited states, and transition elements: Two new functionals and systematic testing of four M06-class functionals and 12 other functionals. *Theor. Chem. Acc.* **2008**, *120*, 215–241. [[CrossRef](#)]
57. Miertuš, S.; Scrocco, E.; Tomasi, J. Electrostatic interaction of a solute with a continuum. A direct utilization of ab initio molecular potentials for the prevision of solvent effects. *Chem. Phys.* **1981**, *55*, 117–129. [[CrossRef](#)]
58. Koopmans, T. Über die Zuordnung von Wellenfunktionen und Eigenwerten zu den einzelnen Elektronen eines Atoms. *Physica* **1934**, *1*, 104–113. [[CrossRef](#)]
59. Parr, R.G. Density functional theory of atoms and molecules. In Proceedings of the Horizons of Quantum Chemistry: Proceedings of the Third International Congress of Quantum Chemistry, Kyoto, Japan, 29 October–3 November 1979; pp. 5–15.

Disclaimer/Publisher’s Note: The statements, opinions and data contained in all publications are solely those of the individual author(s) and contributor(s) and not of MDPI and/or the editor(s). MDPI and/or the editor(s) disclaim responsibility for any injury to people or property resulting from any ideas, methods, instructions or products referred to in the content.